Modeling and Admittance Control of a Piezoactuated Needle Insertion Device for Safe Puncture of Spinal Membranes

Yuzhou Duan
College of Mechanical and Electrical Engineering,
Nanjing University of Aeronautics and Astronautics,
Nanjing 210016, China

Jie Ling[1]
College of Mechanical and Electrical Engineering,
Nanjing University of Aeronautics and Astronautics,
Nanjing 210016, China
e-mail: meejling@nuaa.edu.cn

Yuchuan Zhu[1]
College of Mechanical and Electrical Engineering,
Nanjing University of Aeronautics and Astronautics,
Nanjing 210016, China
e-mail: meeyczhu@nuaa.edu.cn

Robotic-assisted lumbar puncture (LP) has been explored in recent years. The most important step in this procedure is accurately and safely puncturing the spinal membrane (dura mater) based on an automatic needle insertion device (NID). Piezoactuated NID has shown its advantages with high precision and compact structure. Soft control of the NID is important for insertion safety; however, for stick-slip piezoactuated NID, there are few studies due to the complex mechanism of stick-slip motion. Here, a modeling and admittance control method for a proposed stick-slip piezoactuated NID is proposed for safe puncture of the spinal membrane. To analytically model the NID, the compliant mechanism (CM) in the NID is reduced to a second-order system. The stick-slip friction and the spinal membrane are modeled based on the LuGre model and the Hunt–Crossley model, respectively. Based on these models, an admittance controller (AC) for the proposed NID is established to realize the precise control of the position and the safety protection against puncture errors. Simulations and preliminary experiments based on a prototype of the NID and a phantom of the spinal membrane were carried out to test the proposed modeling and control method. Results show that the proposed NID with AC has a maximum insertion error of 0.62 mm and the insertion depth decays by 80% when an unexpected force is applied. Therefore, the proposed model and control method have the potential to be used in real LP procedures by further development.
[DOI: 10.1115/1.4066045]

Keywords: lumbar puncture, stick-slip piezoelectric actuator, robotic-assisted needle insertion, surgical robots

---

1 Introduction

With the development of surgical robots, the surgical form of robotic-assisted lumbar puncture (LP) is being explored [1,2]. In LP and other robotic-assisted needle-based interventions, a needle insertion device (NID) is commonly introduced as the robot's end effector [3–5] to automatically deliver the needle to the specified area. In LP procedure, the most challenging procedure is puncture of the dura mater (the spinal membrane), and avoiding injury to the spinal cord. In comparison with the eardrum in tympanoplasty [6], peritoneum in laparoscopic surgery [7], and other procedures for puncturing membranes, puncturing the spinal membrane in LP is more challenging because it needs to accurately puncture into the dura mater and quickly cease (within 1 mm) to prevent undue harm to the spinal cord [8]. This requires the NID to have good control of insertion force and depth simultaneously, further ensuring the accuracy and safety of the LP procedure. Therefore, the design of the NID and its controller assumes a significantly pivotal role in effectively and precisely governing both the interaction force and needle position.

For the NID design issue, piezo-electric actuation technology possesses considerable advantages of high accuracy and has been adopted in some NIDs recently. According to the working principle, the piezoactuated NID can be classified into two types: inchworm type NID [9] and stick-slip type NID [10]. The actuators of the two types of NIDs are stepping actuators that use specially designed mechanisms to convert finite piezo-electric stroke (usually $\leq 100\,\mu m$) into a theoretically infinite stroke by a repetitive periodic motion of the actuators. The actuator of the inchworm type is a biomimetic actuator that requires multiple piezostacks to realize a complete cycle motion so that the time sequence of the excitation signals is complex. In contrast, the actuator of the stick-slip type can be actuated with a single piezostack so that its structure is relatively compact with simpler driving signals.

Understanding and harnessing the dynamics of the stick-slip piezo-electric actuator are important for structure optimization and controller design. The stick-slip piezo-electric actuators usually involve a piezostack, a compliant mechanism (CM), and the end effector (slider in this paper) interacting with the CM by friction. The dynamic model of the actuator is mostly established by physically equivalent mass-damping-sliding systems. In Ref. [11], based on a linear actuator, a dynamic model considering the stiffness coefficient and damping coefficient of the overall system is introduced. In Ref. [12], a dynamic model of a two-degrees-of-freedom stick-slip microrobot was developed which considered the substep behavior and the stepper mode behavior; an elastoplastic friction model was used to manage the two modes. In Ref. [13], a quasi-static model of the same two-degrees-of-freedom stick-slip microrobot was suggested which was utilized for a single feedback control of both the substep and stepper modes.

Despite the efforts in recent works, there are still difficulties in modeling the actuator adopted in this paper. We have previously developed and tested a novel NID actuated by a stick-slip piezo-electric actuator with a compact structure and competitive performance in device size and insertion resolution [14], as shown in Figs. 1(*a*) and 1(*b*). The difficulties in modeling the proposed actuator lie in the special structure of the CM (the part of the CM in contact with the slider is a flexure joint) and the interaction force between the slider and the driving point (the support force applied to the slider varies with time in the proposed NID).

For the NID control issue, the particularity of puncturing dura mater requires consideration of both the insertion force and position
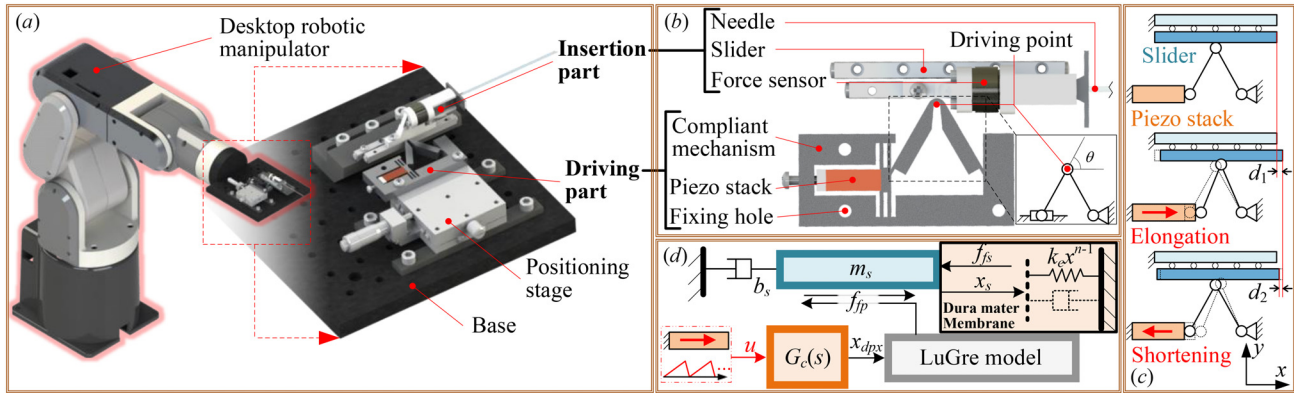
Fig. 1 Schematic diagram of the proposed insertion device: (*a*) device configuration. The needle insertion device is envisaged to be mounted on a desktop robotic manipulator, (*b*) detail of the insertion structure, (*c*) working principle (stick-slip motion) of the needle insertion device, and (*d*) the proposed analytical model of the needle insertion device.

[6]. Impedance and admittance control, proposed by Hogan in 1984 [15], are a fundamental control methodology that is widely adopted in dealing with the dynamic interaction problem between the manipulator and the environment. In comparison with hybrid position and force control, this control module could establish a dynamical relationship between the position and force of the insertion needle and control the ratio of the two parameters [16]. In contrast to impedance control, admittance control shows greater performance in noncontact and low-stiffness tasks [17]. Recently, some advanced admittance controllers for NIDs have been designed. An admittance controller (AC) is developed in Ref. [18] to guarantee the exact force trajectory tracking. In Ref. [19], an admittance control scheme is adopted to maintain sufficient contact force between the ultrasound probe and the human body in kidney stone surgery. In particular, in Ref. [20] a fractional order AC is proposed and possesses the potential ability to suppress the undesirable motion of the needle.

Although some studies have been conducted to develop an AC in NID, the admittance control strategy in stick-slip type NID has not yet been considered. How to control the stick-slip type NID for accurate and safe puncture is still a considerable issue.

This paper proposes the model and admittance control methods of a stick-slip piezoactuated NID for safe puncture of the dura mater. The analytical model and control method are verified through simulations and experiments. The system considered in this paper consists of a designed NID and the dura mater environment. As presented in Fig. 1(*a*), the compact piezoactuated NID is envisaged to be mounted on a desktop robotic manipulator (due to the small mass of the NID). This configuration has the upsides of saving limited surgical space and reducing the risk of human-machine collision. The NID can be mainly divided into two parts: the driving part and the insertion part. As shown in Fig. 1(*b*), the driving part is mounted on an *X*-axis positioning stage so that the preload to the slide of the driving part can be modified. A triangular CM proposed in Ref. [21] is adopted as the transmission mechanism, of which the longitudinal motion of the piezo-electric is translated into the motion of the driving point (the motion direction is expressed by θ). The insertion part integrates a force sensor and a needle mounted on a slider. Figure 1(*c*) introduces the working principle of the stick-slip motion of this NID. The piezostack is actuated by a periodic signal (asymmetric sawtooth wave in this paper) and outputs reciprocating motion of elongation and shortening. Transmitted by the CM, a stick-slip motion is generated at the driving point to drive the slider forward (indicated by d_2-d_1 in one cycle in Fig. 1(*c*)). To achieve a relatively large force output, the NID in Ref. [14] is adopted in this paper. The main contributions of this paper are concluded as follows:

(1) Establishing an analytical model of the stick-slip piezoactuated NID of which the flexure hinge is the driving point.

(2) Proposing an admittance control method compatible with the stick-slip piezoelectric NID to keep the insertion safe.

2 Methods

To achieve safe puncture of the dura mater of the LP procedure, we first establish an analytical model for the proposed stick-slip type piezoactuated NID and the dura mater environment. Then, the AC is designed for the proposed NID for puncture safety. A prototype is fabricated and experiments are designed. Based on the experiments, the proposed model is verified and parameters are identified. Last, the accuracy and safety tests are designed for validation of the feasibility of the proposed method.

2.1 Analytical Model. This subsection establishes the analytical model of the system, including the insertion part, friction, driving part, and dura mater. As shown in Fig. 1(*d*), a mechanics-based mass-damping model is proposed to model the insertion part. The LuGre model is used to model the stick-slip friction between the slider and the driving point [11]. Due to the difficulty of establishing the unconventional flexible hinge in the driving part, this part is considered a second-order system and identified by experiments. To characterize the true force–displacement relationship, the dura mater is established using the nonlinear Hunt–Crossley (H–C) model [22].

2.1.1 Modeling Insertion Part. The insertion part is mounted on the slider, driven by the driving point of the CM, and interacts with the dura mater. In general, the insertion part interacted with the environment can be modeled by the following equation:

$$m_s \ddot{x}_s + b_s \dot{x}_s = f_{\text{fp}} - f_{\text{fs}} - f_e \quad (1)$$

where m_s and b_s are the effective mass and damping coefficient of the slider, x_s is the position measured by the displacement sensor, and $\ddot{x}_s$ is the acceleration of the slider. The spring term is not considered due to the physical reality. f_{fp} is the friction from the driving point of the CM, f_e is the interaction force between needle and dura mater, and f_{fs} is the friction between sliders.

2.1.2 Modeling Friction Force. The LuGre model is adopted to represent the stick-slip friction f_{fp} between the driving point and the slider, where the friction interaction is considered as a contact between bristles. According to Ref. [23], the friction can be modeled as follows:

$$f_{\text{fp}} = \sigma_0 z + \sigma_1 \frac{dz}{dt} + \sigma_2 v$$

$$\frac{dz}{dt} = v - \frac{|v|}{g(v)} z \quad (2)$$

$$\sigma_0 g(v) = f_c + (f_s - f_c) e^{-(v/v_s)^2}$$

where σ_0, σ_1, and σ_2 denote the stiffness, damping coefficient, and viscous friction coefficient of the friction pair, respectively. z is the average deflection of the bristles of the friction pair. $v = v_s - v_{dpx}$ is the relative velocity of slider velocity v_s and x-direction velocity of driving point v_{dpx}. $g(v)$ is a function that depends on material properties, lubrication, etc. v_S denotes the Stribeck velocity. f_s and f_c are the static friction and Coulomb friction, respectively.

ASSUMPTION 1 (see Refs. [23] and [24]). *The friction type is dry friction, and the main source of contribution to z is the preload.*

Therefore, coefficients σ_2 can be omitted, and z can be considered a constant. The simplified version of the LuGre model in this paper can be derived

$$f_{fp} = f_c \text{sgn}(v) + (f_s - f_c)e^{-(v/v_S)^2}\text{sgn}(v) \qquad (3)$$

2.1.3 Modeling Driving Part.
In this part, the driving part of the NID is modeled. Ignoring the nonlinear and inertial effects of the CM and considering the slider as an ideal rigid body, the static friction and Coulomb friction can be modeled as follows:

$$f_s = \mu_s f_N, f_c = \mu_c f_N \qquad (4)$$

$$f_N = \kappa(x_{dpy} + x_{pre}) \qquad (5)$$

where μ_s and μ_c are static and dynamic friction coefficients, respectively. f_N is the support force applied to the slider. κ represents the relationship between the output force and displacement of the driving point. x_{dpy} is the displacement of the driving point in the y-axis direction. x_{pre} is the preload displacement added by the X-axis positioning stage.

Noting that the physical model of the CM is difficult to establish and only the displacement of the driving point is required for LuGre model input, a second-order model is considered to model this system. The input of this system is the applied voltage of the piezostack and the output value is the motion of the driving point. Furthermore, since the displacement in the y-direction is difficult to measure during system identification, the driving point in the x-axis direction (x_{dpx}) is considered as the system output. Regarding the nonlinearity of the mechanical system as disturbance, the driving part can be modeled as follows:

$$G_c(s) = \frac{X_{dpx}(s)}{U(s)} = \frac{k(s - z_1)}{(s - p_1)(s - p_2)} \qquad (6)$$

$$x_{dpy} = x_{dpx}\cot(\theta) \qquad (7)$$

where $G_c(s)$ is the transfer function of the CM system, which has one zero z_1, two poles p_1 and p_2, and the gain is expressed as k. The $X_{dpx}(s)$ and $U(s)$ are the representation of x_{dpx} and input voltage u in the complex domain.

2.1.4 Modeling Dura Mater.
The dura mater has strong viscoelastic, nonlinear, and inhomogeneous properties. Hence, the H–C model is employed in this paper to model the behavior when this soft and thin dura mater is deformed [22,25]. The nonlinear H–C model can be expressed by

$$f_e = \begin{cases} k_e(x_s - x_e)^n & x_s \geq x_e \\ 0 & x_s \leq x_e \end{cases} \qquad (8)$$

where x_e is a constant that denotes the position of the dura mater, $k_e x^n$ demotes the nonlinear elastic force, and n depends on the dura mater material and contact properties. For conciseness, in Fig. 1(d), the value of x_e is set to zero. Of note, the velocity-dependent terms of the model are omitted considering the slow velocity of the slider (≤ 1 mm/s) during insertion.

2.2 Controller Design

2.2.1 Problem Statement.
To carry out the LP by the proposed piezoactuated NID, a controller is required. Some key issues of the controller are discussed in this part. First, although there is an approximately linear relationship between the peak voltage of the driving signal and the puncture speed in the working range of the NID, the positioning error is non-negligible. Additionally, with the increase of the puncture force, the speed of NID will have a certain damping, which is a usual phenomenon in most open-loop actuators. Second, safety is a crucial issue in surgical procedures. In LP surgery, surgeons use the force feedback at the end of the needle to determine the specific condition of the puncture procedure. When the puncture needle is incorrectly estimated and other obstacles (such as bones) are encountered, the controller needs to react to the change in the contact environment.

2.2.2 Admittance Controller Design.
To solve the manipulator-environment interaction problems stated aforementioned, an admittance control scheme for the proposed NID is proposed in Fig. 2. The controller consists of the outer admittance control loop to derive the desired position x_d and the inner motion control loop with a proportional integral differential (PID) controller.

The AC behaves as a mechanical admittance. In this paper, a linear second-order relationship is adopted

$$m_a(\ddot{x}_d - \ddot{x}_r) + b_a(\dot{x}_d - \dot{x}_r) + k_a(x_d - x_r) = f_e \qquad (9)$$

where x_r is the reference trajectory. m_a, b_a, and k_a denote the designed inertia, damping, and stiffness, respectively.

The PID controller is a position controller of the form

$$e_{dc} = k_p e_d + k_i \int_0^t e_d dt + k_d \dot{e}_d \qquad (10)$$

where k_p, k_i, and k_d are positive gains, respectively. $e_d = x_d - x_s$ is the input error and e_{dc} is the control output that denotes the controlled position compensation.

In the experimental part (Sec. 2.3), we verify the approximately linear relationship between velocity and peak voltage of the driving signal, which is described by the electromechanical coupling coefficient T. Thus, the peak voltage u_p can be derived by $u_p = T\dot{e}_{dc}$. Having the peak voltage of the input signal, the programed subsystem sawtooth generator derives the driving signal of the piezostack with the amplitude of u_p, frequency of 1000 Hz, and asymmetry of 90%. The system model established in Sec. 2.1 is represented here as the dynamic plant, where N_s represents the nonlinear dynamic module of the slider and environment.
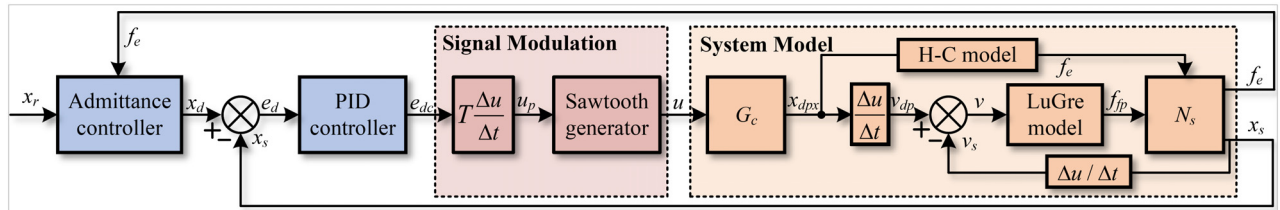

Fig. 2 The overall admittance control scheme of the proposed needle insertion device
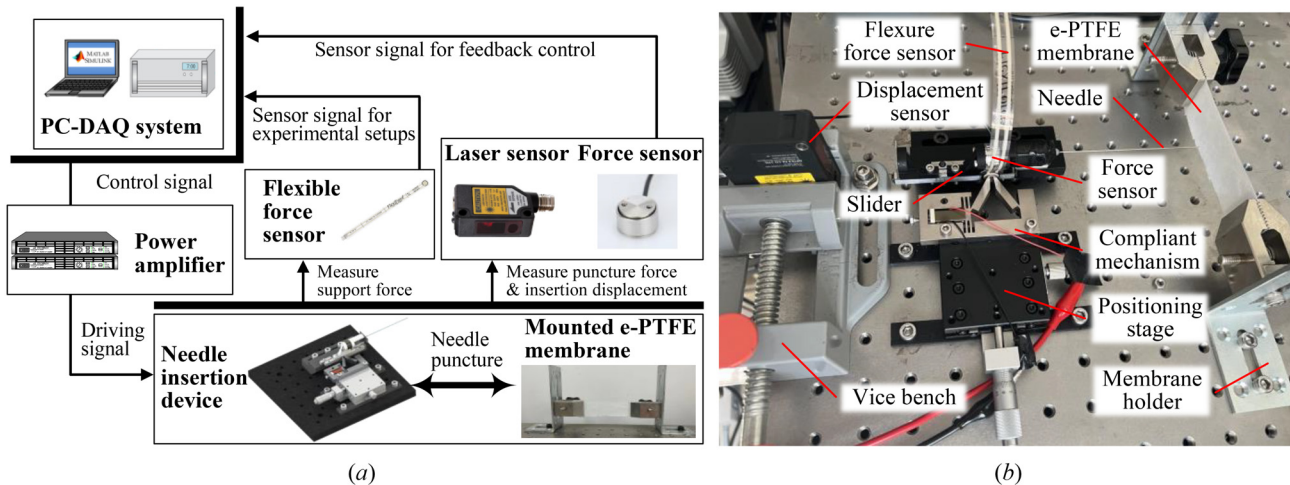
Fig. 3 Experimental system of the proposed needle insertion device and dura mater platform: (a) the signal flow diagram of the experimental system and (b) the prototype of the needle insertion device, the membrane platform, and the sensors

2.3 Experiments

2.3.1 Experimental Setups. Figure 3 presents the experiment system of the piezoactuated NID and the punctured dura mater and the signal flow of the system. Expanded polytetrafluoroethylene (e-PTFE) is adopted as the dura mater-mimetic material due to its similar biomechanical properties [26]. Similar to the real dura mater, the thickness is chosen as $300\,\mu m$. The piezostack (SA070718, Piezo-Drive Co., Ltd., NSW, Australia) is used to drive the triangular CM. The CM of the prototype is made of 45 steel and fabricated via wire-cut electrical discharge machining. The cross-roller slider (VR2-75HX13Z, THK Co., Ltd., Tokyo, Japan) is chosen to guide the needle insertion due to its high stiffness and linearity. The needle force sensor (SBT674 SIMBATOUCH Co., Ltd., Guangzhou, China) is fixed at the bottom of the needle to collect the axial force during insertion. A medical-graded lumbar puncture needle with an outer diameter of 0.7 mm is employed.

A function generator (DG1022U, RIGOL Co., Ltd., Soochow, China) is used to generate the required signal, which is amplified by a power amplifier (7224, AE Techron, Inc., Elkhart, IN) as the input voltage signal of the piezostack. Signals of the force sensor and displacement sensor are collected by a data acquisition card (PCI-6259, NI, Inc., Austin, TX). The asymmetry of the sawtooth wave is set to 90%. Two displacement sensors, a laser sensor (CD33-120NV, OPTEX Co., Ltd., Shiga, Japan) with an accuracy of $120\,\mu m$ and a capacitive displacement sensor (E09.CAP200, Core Tomorrow Co., Ltd., Harbin, China) with a static resolution of 2.5 nm, are used to measure the displacement macroscopically and microscopically. To calibrate the force–displacement ratio κ as well as ensure the consistency of supporting force in each experiment, a flexible piezoresistive force sensor (FlexiForce A201, Tekscan Inc., Norwood, MA) is introduced to measure the supporting force at the driving point.

2.3.2 Model Parameter Determination and Validation. The analytical model has a total of 16 parameters that need to be determined. As shown in Fig. 4(a), a step test under the driven voltage of 40 V is carried out to identify the parameters of the transfer function $G_c(s)$ by using the Matlab system Identification Toolbox. Multiple dura mater puncture experiments are carried out to validate and determine the parameters of the H–C model and the fitting results are shown in Fig. 4(b). The root-mean-square error of the fitted curve is 0.7×10^{-3}. The proposed analytical model is established in the MATLAB/SIMULINK environment, where some unmeasurable parameters are determined by trial-and-error method based on physical reality and experimental data. All the values of the model parameters as well as their source are listed in Table 1.

As presented in Fig. 4(c), the relationship between the amplitude voltage u_p of the driving signal and the slider velocity v_s is

approximately linear under high driving voltage (proofs can be also found in Ref. [21]). Additionally, to guarantee enough insertion force output, the working range of the actuator is limited to high voltage. Therefore, an electromechanical coupling coefficient T is
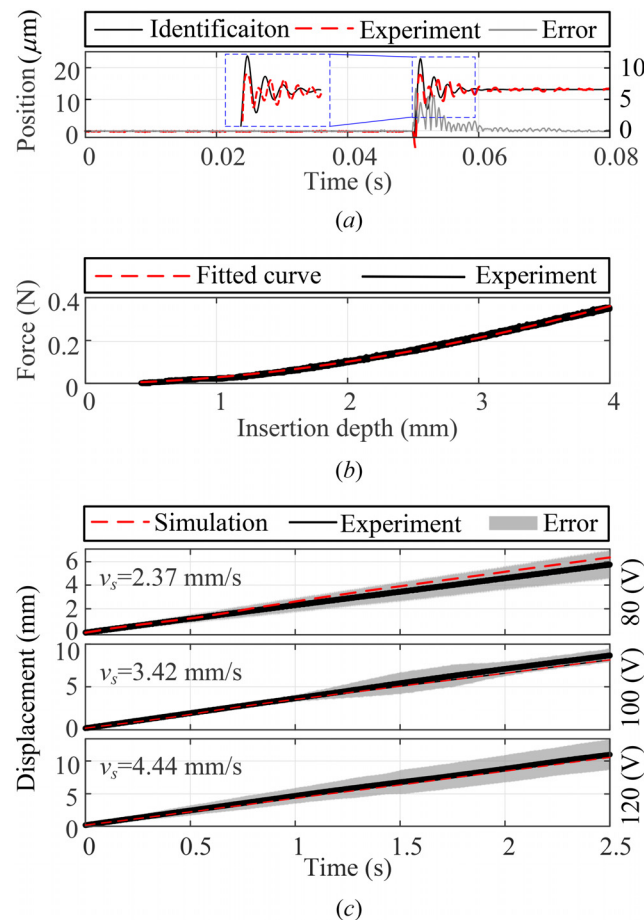

Fig. 4 Experiments for model parameter determination and validation: (a) step test for system identification of $G_c(s)$, (b) the depth-force relationship of needle insertion into the dura mater. The curve is fitted by the Hunt–Crossley model. (c) Comparison of slide/needle displacement between simulated model and experiment under the driving voltage of 80, 100, and 120 V. The gray error band represents ten times the standard deviation of the data for clarity.

Table 1 Determined system parameters and their sources of the proposed analytical model

Parameter	Value	Source
m_s	0.384 kg	Measurement by electronic scales
b_s	0.001 Ns/m	Trail-and-error in MATLAB/SIMULINK
v_S	3.7×10^{-3} m/s	Trail-and-error in MATLAB/SIMULINK
μ_s	0.11	Trail-and-error in MATLAB/SIMULINK
μ_c	0.1	Trail-and-error in MATLAB/SIMULINK
f_{fs}	0.1 N	Trail-and-error in MATLAB/SIMULINK
κ	1.43×10^6 N/m	Identification by force sensor
k	-1.47×10^3	Identification by step experiment
z_1	2.72×10^3	Identification by step experiment
p_1	$(-1.29 + 3.24i) \times 10^3$	Identification by step experiment
p_2	$(-1.29 - 3.24i) \times 10^3$	Identification by step experiment
k_e	0.052	Identification by insertion experiment
x_e	0.5×10^{-3} m	Specified in insertion experiment
n	1.85	Identification by insertion experiment
x_{pre}	1×10^{-4} m	Read by positioning stage
θ	60 deg	Geometric parameter

proposed to describe this almost linear relationship that takes the form $Tv_s = u_p$. The nonlinear error is compensated by the subsequently proposed controller.

The model was tested under the driving frequency of 1000 Hz and voltage of 80, 100, and 120 V to guarantee enough puncture force. Each test was repeated three times to reduce the experiment error.

2.3.3 Method for Accuracy and Safety Tests. For accuracy and safety tests, the proposed AC is established in the MATLAB/SIMULINK environment to preliminarily test the performance. To model the whole procedure of dura mater puncture. An extended H–C model is derived in Fig. 5(*a*) and takes the place of the original H–C model. The controller parameters are tuned by the trial-and-error method. For the accuracy test, the NID is actuated by inputting a reference trajectory of displacement and compared with the PID controller. The given reference signal is a ramp and the slope is the same as the signal in Fig. 4(*c*) under the voltage of 80 V. For the safety test, as shown in Fig. 6, a hypothetical large insertion force (1.5 N) is applied to the axial direction of the needle to simulate the process of incorrect puncture.
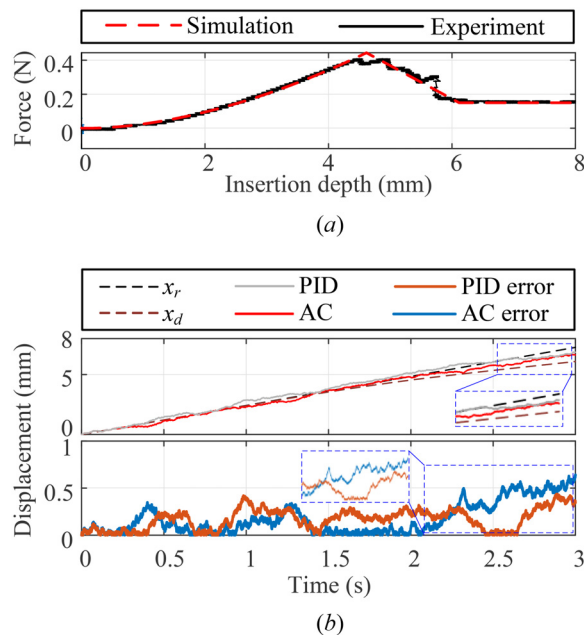
Fig. 5 Accuracy validation of the proposed AC in comparison with PID controller: (*a*) validation of the extended Hunt–Crossley model and (*b*) accuracy validation under a ramp signal
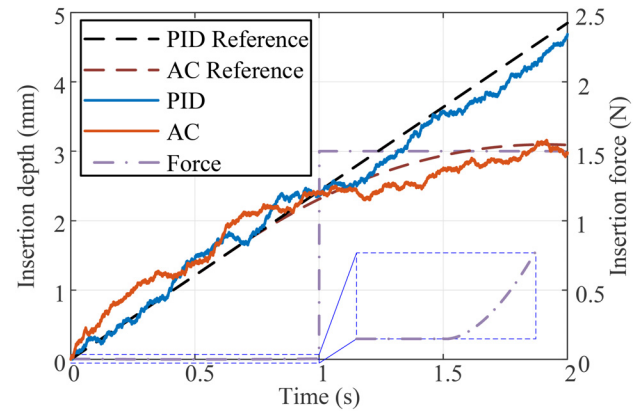
Fig. 6 Incorrect puncture test with a large force to validate the safety of AC in comparison with PID controller

3 Results and Discussion

The model validation results are shown in Fig. 4(*c*), the maximum displacement errors between the analytical model and experiment are 0.27, 0.30, and 0.51 mm under different driving voltages (the maximum error is less than 6.3%). Thus the correctness of the analytical model is validated. Then, based on the model, the control parameters are tuned, as illustrated in Table 2. In the following part of this section, the accuracy and safety tests of AC are conducted and the results are presented in this section in comparison with PID. Discussion of the experimental results is made as well as the further development of the proposed NID.

3.1 Results

3.1.1 Accuracy Test. The results of the accuracy test are presented in Fig. 5(*b*), of which the reference signal x_r, desired signal x_d, the controlled outputs of the PID and AC, and the errors are illustrated. The information from the enlarged part of the figure shows the error of the AC will be slightly larger than the error of the PID controller as the insertion force increases (due to the difference of reference signal x_d and x_r). The insertion accuracy is defined by the maximum error between the reference trajectory and the real trajectory measured by the sensor. In this way, the insertion accuracy can be used to represent the insertion error after puncturing the membrane. The results show that the error difference between the two controllers is not significant in a normal puncture procedure, and for both two controllers, the maximum errors are less than 0.62 mm (less than 1 mm for dura mater puncture [8]). Thus, the insertion accuracy can be guaranteed.

3.1.2 Safety Test. As shown in Fig. 6, the results illustrate that the PID controller keeps tracking the reference signal while the AC behaves as a damping in insertion depth. The results showed that the introduction of AC could improve the safety during needle insertion; however, additional bench tests using a realistic spine model are needed for further validation of the safety.

3.2 Discussion. The results of accuracy and safety tests have preliminarily illustrated the effectiveness of the AC in piezoactuated NID when an e-PTFE membrane is considered as the dura membrane. First, the accuracy of NID in puncturing the e-PTFE

Table 2 Parameters of the proposed controller

Parameter	value	Parameter	value
k_p	0.29	m_a	1
k_i	0.5×10^{-3}	b_a	0.01
k_d	0.5×10^{-5}	k_a	0.1

(dura mater-mimetic material) is validated in comparison with the conventional PID controller. Then, the safety issue is considered by introducing a common iatrogenic error, i.e., failure to enter the ligaments between lumbar vertebrae. Our ultimate goal is to develop a compact, accurate, and safe piezoactuated NID for the robotic-assisted LP. As shown in Fig. 1(*a*), we envisage the proposed NID could be mounted on a desktop robotic manipulator so that it could save limited surgical space and reduce the risk of human-machine collision. Works including improvement of the reliability of the stick-slip actuator and development of the procedure-compliant high-level controller still needs to be handled.

There is still a lot of work to be done to achieve the productization of the proposed piezoactuated NID together with the modeling and control method. Of the 16 parameters listed in Table 1, 13 of them are NID-related, which can be identified offline and remain unchanged. The other three parameters are membrane-related, that is, k_e, x_e, and n, the method of online identification is required because of the specificity of different human tissues for safety considerations.

4 Conclusions

Robotic-assisted LP has been explored in recent years, and piezoactuated NID has received considerable critical attention. The stick-slip piezo-electric actuator has the most compact and lightest structure, which enables the driven NID to be installed on a desktop robotic manipulator. In this work, we have preliminary verified the safety and accuracy of using a stick-slip piezoactuated NID for membrane puncture based on the modeling and control method. Local system identification is adopted for modeling the triangular CM with a flexible hinge as the driving point. An admittance control method compatible with the stick-slip piezo-electric actuator is proposed to maintain insertion accuracy and puncture safety simultaneously. Studies, including LP phantom tests and collaborative drives with desktop-level robotic arms, need to be carried out for further development.

Funding Data

Data Availability Statement

No data, models, or code were generated or used for this paper.

Nomenclature

Abbreviations

AC = admittance controller
CM = compliant mechanism
e-PTFE = expanded polytetrafluoroethylene
H–C = Hunt–Crossley
LP = lumbar puncture
NID = needle insertion device

References

[1] Duan, Y., Ling, J., Feng, Z., Yao, D., and Zhu, Y., 2024, "Development of a Base-Actuated Three-Rhombus Configured Remote Center of Motion Mechanism for Lumbar Puncture," ASME J. Mech. Rob., **16**(5), p. 054503.
[2] Gao, C., Phalen, H., Margalit, A., Ma, J. H., Ku, P. C., Unberath, M., Taylor, R. H., Jain, A., and Armand, M., 2022, "Fluoroscopy-Guided Robotic System for Transforaminal Lumbar Epidural Injections," IEEE Trans. Med. Rob. Bionics, **4**(4), pp. 901–909.
[3] Li, J., and Jiang, Q., 2023, "Optimal Design and Experiment of Cable-Driven Puncturing Surgery Robot for Soft Needle," ASME J. Med. Devices, **17**(2), p. 021008.
[4] McDonald, R. C., 2022, "Development of a pO2-Guided Fine Needle Tumor Biopsy Device," ASME J. Med. Devices, **16**(2), p. 021003.
[5] Duan, Y., Ling, J., Feng, Z., Ye, T., Sun, T., and Zhu, Y., 2024, "A Survey of Needle Steering Approaches in Minimally Invasive Surgery," Ann. Biomed. Eng., **52**(6), pp. 1492–1517.
[6] Feng, Z., Liang, W., Ling, J., Xiao, X., Tan, K. K., and Lee, T. H., 2022, "Adaptive Robust Impedance Control for an Ear Surgical Device With Soft Interaction," IEEE/ASME Trans. Mechatron., **27**(3), pp. 1784–1795.
[7] Du, Z., Liang, Y., Yan, Z., Sun, L., and Chen, W., 2021, "Human-Robot Interaction Control of a Haptic Master Manipulator Used in Laparoscopic Minimally Invasive Surgical Robot System," Mech. Mach. Theory, **156**, p. 104132.
[8] Holton, L. L. H., 2000, "Development of a Haptic Feedback Model for Computer Simulation of the Epidural Anesthesia Needle Insertion Procedure," The Ohio State University, Columbus, OH.
[9] El Bannan, K., Chronik, B. A., and Salisbury, S. P., 2015, "Development of an MRI-Compatible Compact, Rotary-Linear Piezoworm Actuator," ASME J. Med. Devices, **9**(1), p. 014501.
[10] Deng, J., Liu, S., Liu, Y., Wang, L., Gao, X., and Li, K., 2022, "A 2-DOF Needle Insertion Device Using Inertial Piezoelectric Actuator," IEEE Trans. Ind. Electron., **69**(4), pp. 3918–3927.
[11] Wang, X., Zhu, L., and Huang, H., 2021, "A Dynamic Model of Stick-Slip Piezoelectric Actuators Considering the Deformation of Overall System," IEEE Trans. Ind. Electron., **68**(11), pp. 11266–11275.
[12] Rakotondrabe, M., Haddab, Y., and Lutz, P., 2009, "Development, Modeling, and Control of a Micro-/Nanopositioning 2-DOF Stick–Slip Device," IEEE/ASME Trans. Mechatron., **14**(6), pp. 733–745.
[13] Rakotondrabe, M., Haddab, Y., and Lutz, P., 2008, "Voltage/Frequency Proportional Control of Stick-Slip Micropositioning Systems," IEEE Trans. Control Syst. Technol., **16**(6), pp. 1316–1322.
[14] Duan, Y., Peng, H., Zhu, Y., Shen, Y., and Ling, J., 2023, "Inertial Piezoelectric Actuation of a Needle Insertion Device for Minimally Invasive Surgery," Proceedings of the 2023 IEEE International Conference on Robotics and Biomimetics (ROBIO), Koh Samui, Thailand, Dec. 4–9, pp. 1–6.
[15] Hogan, N., 1984, "Impedance Control: An Approach to Manipulation," Proceedings of the 1984 American Control Conference, San Diego, CA, June 6–8, pp. 304–313.
[16] Ott, C., Mukherjee, R., and Nakamura, Y., 2010, "Unified Impedance and Admittance Control," Proceedings of the 2010 IEEE International Conference on Robotics and Automation, Anchorage, AK, May 3–7, pp. 554–561.
[17] Cousin, C. A., 2020, "Adaptive Admittance Control of Hybrid Exoskeletons," Proceedings of the 2020 American Control Conference (ACC), Denver, CO, July 1–3, pp. 545–550.
[18] Li, H., Nie, X., Duan, D., Li, Y., Zhang, J., Zhou, M., and Magid, E., 2022, "An Admittance-Controlled Amplified Force Tracking Scheme for Collaborative Lumbar Puncture Surgical Robot System," Int. J. Med. Rob. Comput. Assisted Surg., **18**(5), p. e2428.
[19] Paranawithana, I., Li, H.-Y., Foong, S., Tan, U.-X., Yang, L., Lim, T. S. K., and Ng, F. C., 2018, "Ultrasound-Guided Involuntary Motion Compensation of Kidney Stones in Percutaneous Nephrolithotomy Surgery," Proceedings of the 2018 IEEE 14th International Conference on Automation Science and Engineering (CASE), Munich, Germany, Aug. 20–24, pp. 1123–1129.
[20] Aydin, Y., Tokatli, O., Patoglu, V., and Basdogan, C., 2018, "Stable Physical Human-Robot Interaction Using Fractional Order Admittance Control," IEEE Trans. Haptics, **11**(3), pp. 464–475.
[21] Zhang, Y., Peng, Y., Sun, Z., and Yu, H., 2019, "A Novel Stick–Slip Piezoelectric Actuator Based on a Triangular Compliant Driving Mechanism," IEEE Trans. Ind. Electron., **66**(7), pp. 5374–5382.
[22] Feng, Z., Liang, W., Ling, J., Xiao, X., Tan, K. K., and Lee, T. H., 2022, "Precision Force Tracking Control of a Surgical Device Interacting With a Deformable Membrane," IEEE/ASME Trans. Mechatron., **27**(6), pp. 5327–5338.
[23] De Wit, C. C., Olsson, H., Astrom, K. J., and Lischinsky, P., 1995, "A New Model for Control of Systems With Friction," IEEE Trans. Autom. Control, **40**(3), pp. 419–425.
[24] Huo, Z., Tian, Y., Wang, F., Zhang, W., Shi, B., and Zhang, D., 2022, "A Dual-Driven High Precision Rotary Platform Based on Stick-Slip Principle," IEEE/ASME Trans. Mechatron., **27**(5), pp. 3053–3064.
[25] Aydın, H. E., Kızmazoglu, C., Kaya, I., Husemoglu, B., Sozer, G., Havıtcıoglu, H., and Arslantas, A., 2019, "Biomechanical Properties of the Cranial Dura Mater With Puncture Defects: An In Vitro Study," J. Korean Neurosurg. Soc., **62**(4), pp. 382–388.
[26] Kizmazoglu, C., Aydin, H. E., Kaya, I., Atar, M., Husemoglu, B., Kalemci, O., Sozer, G., and Havitcioglu, H., 2019, "Comparison of Biomechanical Properties of Dura Mater Substitutes and Cranial Human Dura Mater: An In Vitro Study," J. Korean Neurosurg. Soc., **62**(6), pp. 635–642.